Roper, S.M. and Lister, J.R. (2005) *Buoyancy-driven crack propagation from an over-pressured source.* Journal of Fluid Mechanics, 536 . pp. 79-98. ISSN 0022-1120

http://eprints.gla.ac.uk/13289/

Deposited on: 12 February 2010

Enlighten – Research publications by members of the University of Glasgow
http://eprints.gla.ac.uk

J. Fluid Mech. (2005), *vol.* 536, *pp.* 79–98. © 2005 Cambridge University Press
doi:10.1017/S0022112005004337 Printed in the United Kingdom

Buoyancy-driven crack propagation from an over-pressured source

By S. M. ROPER AND J. R. LISTER

Institute of Theoretical Geophysics, Department of Applied Mathematics and Theoretical Physics, University of Cambridge, Wilberforce Road, Cambridge, CB3 0WA, UK

(Received 15 October 2004 and in revised form 8 February 2005)

The propagation of a liquid-filled crack from an over-pressured source into a semi-infinite uniform elastic solid is studied. The fluid is lighter than the solid and propagates due to its buoyancy and to the source over-pressure. The role of this over-pressure at early and late times is considered and it is found that the combination of buoyancy and over-pressure leads to significantly different behaviour from buoyancy or over-pressure alone. Lubrication theory is used to describe the flow, where the pressure in the fluid is determined by the elastic deformation of the solid due to the presence of the crack. Numerical results for the evolution of the crack shape and speed are obtained. The crack grows exponentially at early times, but at later times, when buoyancy becomes important, the crack growth accelerates towards a finite-time blow-up. These results are explained by asymptotic similarity solutions for early and late times. The predictions of these solutions are in close agreement with the full numerical results. A different case of crack geometry is also considered in order to highlight connections with previous work. The geological application to magma-filled cracks in the Earth's crust, or dykes, is discussed.

1. Introduction

The transport of magma from deep regions in the Earth to shallower regions occurs through several mechanisms. In the mantle, magma is formed when the solid rock partially melts. This melting can occur by an increase in the temperature, but more commonly by a decrease in the pressure due to mantle upwelling or by a change in the composition due to a flux of volatiles such as water. The magma is less dense than the parent rock and percolates up through the matrix of unmolten minerals, driven by its buoyancy. It collects into veins and then pools in reservoirs at the base of the crust. These magma chambers can be kilometres in size. Evidence for the presence of magma chambers deep in the Earth comes from inverting seismic signals to show regions of lower velocity, indicating the presence of melt.

Differential stress caused by the buoyancy and pressure of the melt and local tectonic stresses causes cracks to open and propagate from the chamber. The cracks are called dykes when they intrude in a vertical plane and sills when they intrude in a horizontal plane. The propagation of dykes corresponds to a flux of mass and heat from the mantle to and through the crust, which has a significant effect on the evolution of the Earth's crust, as well as contributing to the Earth's surface volcanism. The dramatic 'curtains of fire' seen in places like Hawaii and Iceland are examples of dykes breaking through the Earth's surface. Dykes solidify as they cool on a time scale of days, and may be exposed millions of years later as the surrounding

rock is eroded over time. An excellent review by Rubin (1995*b*) covers the geological background to the problem of dyke propagation and describes the main physical features of dykes, in particular that they are near-planar sheets of magma propagating a fracture in the regime of linear elastic fracture mechanics, away from a reservoir of magma.

Various solutions for fluid-driven fracture have been derived in previous work. Weertman (1971) demonstrated that a sufficiently large buoyant fluid-filled crack would begin to propagate upwards but did not calculate the effects of viscous flow in the crack. Spence & Sharp (1985) obtained similarity solutions for a fluid-driven crack that propagates symmetrically in an infinite solid from an over-pressured source, but without buoyancy. They specified the flux of fluid into the crack, and found that for fluxes with a power-law time-dependence the pressure at the origin also has power-law time-dependence, while for fluxes with an exponential time-dependence the over-pressure at the source (in the centre of the symmetric crack) remains constant. This conclusion can be inverted so that a specified constant over-pressure at the source will imply exponential crack growth in the absence of buoyancy. Lister (1990*b*) and Spence, Sharp & Turcotte (1987) considered the effect of buoyancy on a crack which propagates fed by a constant flux of fluid. They found travelling-wave solutions in which the flux of fluid into the crack is an input parameter that sets the propagation speed. The shape of the crack can be divided into a bulbous head, in which buoyancy and elastic pressure are both important, and a constant-width tail, where the over-pressure decays with distance from the crack tip and the flow is simply driven by buoyancy. In geological applications it seems more appropriate to specify the source over-pressure instead of the flux.

Mériaux & Jaupart (1998) considered propagation driven by buoyancy and a specified over-pressure through an elastic plate of finite thickness and found numerical solutions for the crack opening and speed. Their numerical solutions showed that the crack widened continually at its base and developed a head-and-tail structure, thus showing an amalgam of the features of the solutions of Spence & Sharp (1985) and Lister (1990*b*). It was not clear how much of this behaviour should be attributed to the decreasing rigidity of the plate as the crack approached the upper surface. The propagation of a liquid-filled crack with buoyancy and over-pressure has also been the subject of recent experiments by Menand & Tait (2002). They these considered fractures in gelatin, driven by water from a reservoir at constant pressure beneath the gelatin. Although their experiments involved fully three-dimensional cracks with a finite lateral extent, they also comment on the development of a bulbous head fed by a narrow tail. They developed scaling arguments for their results and noted that the experimental parameters were such that the rate of propagation was controlled by the strength of the gelatin rather than the viscosity of the fluid. Other experimental studies in gelatin have incorporated such effects as interaction between multiple fractures (Ito & Martel 2002) and the focusing of fracture paths by external loading (Muller, Ito & Martel 2001). Other features of magma-driven propagation, such as the existence of vapour at the crack tip (Lister 1990*b*; Garagash & Detournay 1998), the solidification of magma as it cools (Lister 1994*a*, *b*; Rubin 1995*a*; Bolchover & Lister 1999), non-Newtonian rheology (Adachi & Detournay 2002) and dyke ascent through partially molten rock (Rubin 1998), have been also studied. A related body of literature concerns hydro-fracture (e.g. Perkins & Kern 1961; Nordgren 1972; Geertsma & Haafkens 1979; Huang, Szewczyk & Li 1990; Atkinson & Thiercelin 1993) which is of great interest to the oil industry, particularly when the porous nature of the rock is taken into account (e.g. Atkinson & Craster 1991).

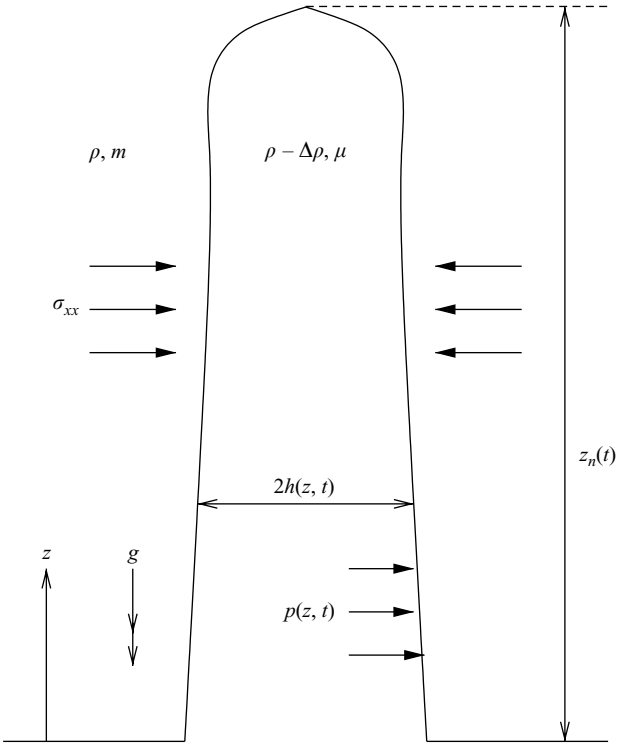

FIGURE 1. Definition sketch. The width of the crack has been exagerated for clarity.

The case of a crack propagating under the influence of both buoyancy and over-pressure in an infinite impermeable solid has not been considered analytically, as pointed out in Rubin (1995*b*). In this paper we consider such propagation, first deriving the governing equations in § 2, then developing scaling arguments in § 3 which we use both to simplify the equations and to inform a numerical study of the solutions in § 4. We then explain the features of the solutions using asymptotic similarity solutions in § 5 and § 6, and finally discuss the relevance of the results in § 7.

2. Formulation of the problem

Consider a two-dimensional crack propagating into a semi-infinite uniform elastic solid occupying $z \geqslant 0$ from a reservoir of fluid occupying $z < 0$, where z is the vertical coordinate, as shown in figure 1. The plane of the crack is assumed to be vertical. Let the solid have density ρ, shear modulus G and Poisson's ratio ν, and define an elastic modulus $m = G/(1-\nu)$. Let the half-width of the crack be $h(z,t)$, $0 < z < z_n(t)$, where the crack tip is at $z = z_n(t)$. Let the crack be filled with viscous fluid of density $\rho - \Delta\rho$ and viscosity μ, so that the fluid is driven upwards by buoyancy $\Delta\rho g$, with gravity g acting downwards. We also assume that the pressure at the top of the reservoir is ΔP greater than the horizontal stress in the solid just above the reservoir.

2.1. *Fluid mechanics*

The flow of viscous fluid in the crack is driven by the gradient of the fluid pressure $p(z)$ and by buoyancy $\Delta\rho g$. The pressure $p(z)$ is equal to the sum of the ambient stress in the solid prior to crack propagation and the elastic stress due to the deformation

of the crack walls. The aspect ratio of a crack, width to length, is given in order of magnitude by the ratio of typical elastic over-pressures to the elastic modulus of the solid, see § 3. In the Earth this gives dykes with aspect ratios in the range 10^{-2}–10^{-4}, which is to say that the cracks are long and thin.

The long thin geometry of the fluid flow, together with the high viscosity of magma, means that the flow in the crack is described well by lubrication theory provided that the modified Reynolds number is small. If this condition is satisfied then the flux of fluid in the crack is given by

$$q = -\frac{2h^3}{3\mu}\left(\frac{\partial p}{\partial z} + (\rho - \Delta\rho)\, g\right). \tag{2.1}$$

With the equation of continuity, $\nabla \cdot \boldsymbol{u} = 0$, (2.1) yields the usual Reynolds equation

$$\frac{\partial (2h)}{\partial t} = -\frac{\partial q}{\partial z} = \frac{2}{3\mu}\frac{\partial}{\partial z}\left(h^3\left(\frac{\partial p}{\partial z} + (\rho - \Delta\rho)\, g\right)\right) \tag{2.2}$$

to describe the evolution of the width of the crack.

The fluid pressure is given by $p = p_e - \sigma_{xx}$, where $p_e(z)$ is the pressure due to elastic deformation by the presence of the crack and σ_{xx} is the ambient horizontal stress in the solid prior to crack propagation. The ambient stress σ_{xx} is given by $\sigma_{xx} = \rho g z + \Delta\sigma$ (Rubin 1995*b*), where $\Delta\sigma$ is the deviation from lithostatic stress due to regional tectonic deformation. Some tectonic stress $\Delta\sigma$ is usually needed to initiate the crack and determine the plane of propagation. For simplicity we assume that $\Delta\sigma$ is linear in the vertical coordinate z so that it can be absorbed into an apparent, or modified, solid density defined by $\rho g = \mathrm{d}\sigma_{xx}/\mathrm{d}z$. The Reynolds equation (2.2) then becomes

$$\frac{\partial h}{\partial t} = \frac{1}{3\mu}\frac{\partial}{\partial z}\left(h^3\left(\frac{\partial p_e}{\partial z} - \Delta\rho g\right)\right). \tag{2.3}$$

A boundary condition is imposed at the tip of the crack to ensure that there is no source or sink of mass there. Balancing fluxes, $q = h\dot{z}_n$, gives

$$3\mu\dot{z}_n = -\lim_{z \to z_n} h^2 \frac{\partial p_e}{\partial z} \tag{2.4}$$

where $h \to 0$ and $\partial p_e/\partial z \to -\infty$ are evaluated at the crack tip.

The boundary condition at the base of the crack, $z = 0$, is that the source over-pressure is ΔP larger than the stress in the solid just above the source. Thus

$$p_e(0) = \Delta P. \tag{2.5}$$

2.2. *Solid mechanics*

Provided the displacement gradients are small, $\partial h/\partial z \ll 1$, we may use linear elasticity to describe the solid mechanics. As expected from a linear theory of elasticity, the elastic pressure is a linear functional of the crack opening. The elastic pressure $p_e(z)$ can be related to the crack half-width h via a Hilbert-like transform

$$p_e(z) = -\frac{m}{\pi}\int_L \frac{\partial h}{\partial s} k(s, z)\, \mathrm{d}s \tag{2.6}$$

using, for example, a Green's function approach or complex-variable methods. The kernel, $k(s, z)$, in (2.6) depends on the crack geometry and the boundary conditions on the solid; L is the crack domain.

Spence & Sharp (1985) used

$$k_{SS}(s, z) = \frac{1}{s-z} + \frac{1}{s+z}, \tag{2.7}$$

which describes a symmetric crack in an infinite solid. Since the Green's function solution for a point dislocation at s (i.e. a point discontinuity in the displacement field) is $1/(s-z)$, we can interpret k_{SS} as the sum of a point dislocation at s and another at $-s$, appropriate to the symmetry.

For the case where the crack propagates into a half-space away from a fluid reservoir so that the boundary of the solid is traction-free, the relevant kernel is

$$\begin{aligned} k_{TF}(s, z) &= \frac{1}{s-z} - \frac{s^2 - 4sz - z^2}{(s+z)^3} \\ &= \frac{1}{s-z} - \frac{1}{s+z} + \frac{6z}{(s+z)^2} - \frac{4z^2}{(s+z)^3} \end{aligned} \tag{2.8}$$

(Broberg 1999, pp. 152–156). In k_{TF}, we have the sum of a dislocation at s, an equal and opposite dislocation at $-s$ and other terms to make the boundary $z=0$ stress free. This expression is reminiscent of Lorentz's image system for Stokes flow (Lorentz 1907), reflecting the fact that both the Airy stress function in plane elasticity and the streamfunction in Stokes flow satisfy the biharmonic equation.

In this paper, we will mainly consider the kernel (2.8) to give the fluid pressure in (2.6), though we will present some calculations with (2.7) to establish a connection with the results of Spence & Sharp (1985).

2.3. *Fracture mechanics*

For slender cracks, linear elasticity predicts a singularity in the stress field ahead of the crack tip of the form $K_I/r^{1/2}$, where r is the distance from the tip. The coefficient K_I is called the mode-I stress-intensity factor and its magnitude depends on both the crack opening and the boundary conditions on the solid. The fact that the stress field near the tip is dominated by this singularity motivates a propagation criterion that the tip will extend if $K_I \geqslant K_c$, where K_c is a material property known as the critical stress-intensity factor (or fracture toughness). This criterion can also be related to the conversion of elastic potential energy to new surface energy as the crack extends (Lawn & Wilshaw 1975). For fluid-driven propagation controlled by the rate of viscous flow rather than by the wave speed in the solid, the crack propagates in the marginal state $K_I = K_c$.

The condition that $K_I = K_c$ can be rewritten

$$h \sim \frac{K_c}{m} \left(\frac{2}{\pi} (z_n - z) \right)^{1/2} \quad \text{as } z \to z_{n-}. \tag{2.9}$$

Equation (2.9) can further be written as an integral constraint on $p_e(z)$ for $z \in L$ if the integral relation (2.6) can be inverted.

2.4. *Summary*

Equations (2.3)–(2.9) describe the propagation of a crack into a half-space from a reservoir of fluid. We have used lubrication theory (2.3), elasticity (2.6), and fracture mechanics (2.9). Together with boundary conditions for the tip of the crack (2.4), and the base of the crack (2.5), these equations constitute an intriguing form of lubrication problem in which the pressure is non-locally determined by the integral equation (2.6).

This non-local pressure arises in other problems in fluid-driven fracture and makes them unlike most lubrication problems in which the fluid pressure is derived from the local film thickness, interfacial curvature, etc.

3. Scalings and non-dimensionalization

By considering (2.3), we can identify several dynamical regimes through which the crack passes as it propagates. We assume that the over-pressure remains of size ΔP over the length of the crack during propagation. As the crack length z_n increases, the scale $\Delta\rho g z_n$ of the buoyancy pressure increases, the over-pressure ΔP remains constant and the scale of the fracture pressure $K/z_n^{1/2}$ decreases. Hence initially, for $z_n \ll (K/\Delta P)^2$ the propagation is controlled primarily by resistance to fracture. For $(K/\Delta P)^2 \ll z_n \ll \Delta P/\Delta\rho g$ the propagation is driven primarily by the over-pressure at the source. Finally, for $z_n \gg \Delta P/\Delta\rho g$ the propagation is driven primarily by buoyancy, but in such a way as to keep the over-pressure constant. This sequence of propagation regimes assumes that $K \ll \Delta P\,(\Delta P/\Delta\rho g)^{1/2}$, so that the fracture-controlled regime finishes before the buoyancy-controlled regime begins as the crack length increases. For typical geological parameters (see Lister & Kerr 1991), the fracture-controlled regime lasts for only order tens of metres, after which we may neglect the strength of the rock and set $K_c = 0$. The transition from the regime of over-pressure-driven propagation to the regime of buoyancy-driven propagation occurs on a scale of several hundreds of metres to a few kilometres and will be the focus of our investigation here. We refer to the transition length $\Delta P/\Delta\rho g$ as the buoyancy length.

The constant source over-pressure suggests the scaling $p_e \sim \Delta P$ which, from (2.6), suggests that $h \sim \Delta P z_n/m$. The natural vertical length scale is the buoyancy length $\Delta P/\Delta\rho g$ at which over-pressure and buoyancy are comparable and $h \sim \Delta P^2/\Delta\rho g m$. At this length the viscous time scale $\mu z_n^2/h^2\Delta P$ estimated from (2.3) is $t \sim \mu m^2/\Delta P^3$. Using these scalings, we define dimensionless variables

$$P = \frac{p_e}{\Delta P}, \tag{3.1}$$

$$H = \frac{m}{\Delta P}\,\frac{h}{z_n}, \tag{3.2}$$

$$Z_n = \frac{\Delta\rho g}{\Delta P}\,z_n, \tag{3.3}$$

$$\tau = \frac{\Delta P^3}{\mu m^2}\,t. \tag{3.4}$$

We also map the time-dependent extent of the crack onto the fixed domain $[0, 1]$ by defining

$$\zeta = \frac{z}{z_n(t)}. \tag{3.5}$$

With the scalings (3.1)–(3.5), the governing equations (2.3)–(2.9) become

$$\frac{\partial H}{\partial \tau} + \left(H - \zeta\frac{\partial H}{\partial \zeta}\right)\frac{1}{Z_n}\frac{\mathrm{d}Z_n}{\mathrm{d}\tau} = \frac{1}{3}\frac{\partial}{\partial\zeta}\left(H^3\left(\frac{\partial P}{\partial\zeta} - Z_n\right)\right), \tag{3.6}$$

$$P(\zeta) = -\frac{1}{\pi}\int_0^1 \frac{\partial H}{\partial s}k(s,\zeta)\,\mathrm{d}s, \tag{3.7}$$

$$\frac{3}{Z_n}\frac{\mathrm{d}Z_n}{\mathrm{d}\tau} = \lim_{\zeta\to 1} H^2\left(Z_n - \frac{\partial P}{\partial \zeta}\right), \tag{3.8}$$

$$P(0) = 1, \tag{3.9}$$

$$H(1-\zeta)^{-1/2} \to 0 \quad \text{as } \zeta \to 1. \tag{3.10}$$

Although $H \to 0$ as $\zeta \to 1$, we retain the term $H^2 Z_n$ for notational convenience in the limit on the right-hand side of (3.8). The extra terms on the left-hand side of (3.6) arise from the time-dependent scaling of both the vertical coordinate and the crack half-width with $z_n(t)$.

4. Time-dependent calculations

In this section we describe the numerical scheme used to solve (3.6)–(3.10) and show the results of the time-dependent calculations. The observed behaviour will be investigated further and asymptotic similarity solutions derived in § 5 and § 6.

4.1. *Numerical scheme*

We split the domain [0, 1] occupied by the crack into N equal panels and represent H by a spline through the N values at the mid-points of the panels. The form of spline chosen is $(1-\zeta)^{1/2}$ multiplied by a piecewise quadratic function that is continuous and has continuous derivative. This form was chosen so that the stress-intensity condition (3.10) can easily be applied. To specify the spline we use the N mid-point values of H, $2N-2$ continuity conditions at joins between panels and two neutral conditions on the derivative of the spline at the end points of the interval [0, 1]. The spline is used to obtain the values of H at the end points of the panels and also to calculate the pressure at the mid-points from (3.7). The integrals of the quadratic spline in (3.7) are found analytically.

We note that (3.6) can be written as

$$\frac{\partial H}{\partial \tau} = -\frac{2H}{Z_n}\frac{\mathrm{d}Z_n}{\mathrm{d}\tau} + \frac{\partial}{\partial \zeta}\left(\frac{1}{3}H^3\left(\frac{\partial P}{\partial \zeta} - Z_n\right) + \frac{\zeta H}{Z_n}\frac{\mathrm{d}Z_n}{\mathrm{d}\tau}\right) \tag{4.1}$$

and define a flux

$$-Q = \frac{1}{3}H^3\left(\frac{\partial P}{\partial \zeta} - Z_n\right) + \frac{\zeta H}{Z_n}\frac{\mathrm{d}Z_n}{\mathrm{d}\tau}, \tag{4.2}$$

which we calculate at the end points of the panels. The required end-point values of $\partial P/\partial \zeta$ are generally obtained using centred differences on the mid-point values of P. At $\zeta = 0$ we use the mid-point values of P for the first two panels together with the boundary condition $P(0) = 1$ to calculate $\partial P/\partial \zeta$ at $\zeta = 0$. At $\zeta = 1$ the boundary condition is that there is no source or sink of mass, i.e. $Q = 0$. The time derivative of H is found using the centred difference

$$\Delta\zeta\left(\frac{\partial H}{\partial \tau} + \frac{2H}{Z_n}\frac{\mathrm{d}Z_n}{\mathrm{d}\tau}\right) = -Q\left(\zeta + \tfrac{1}{2}\Delta\zeta\right) + Q\left(\zeta - \tfrac{1}{2}\Delta\zeta\right), \tag{4.3}$$

from which the values of H can be updated using an explicit Euler time step once the rate of propagation $\dot{Z}_n$ is known. This scheme is second-order accurate in space and first-order in time. Equation (4.1) has an advective term and a diffusive term so the usual conditions for stability apply and, on considering the coefficients of the advective and diffusive terms, it is found necessary to vary the time step with $\Delta\tau \sim 1/Z_n$.

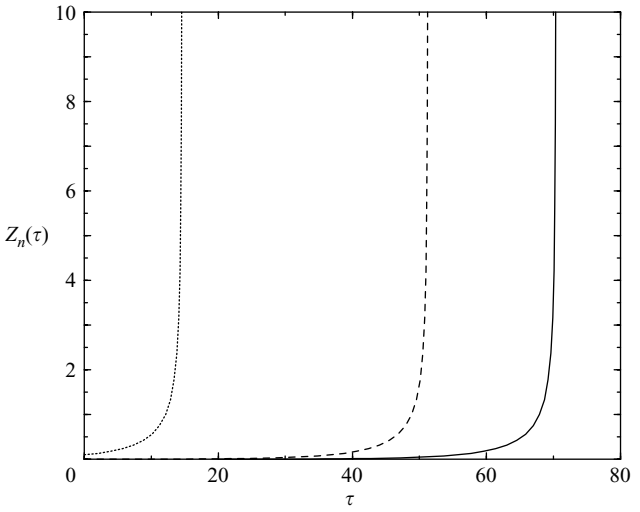

FIGURE 2. Dimensionless length Z_n as a function of time τ, for $Z_n(0) = 10^{-1}$ (dotted), $Z_n(0) = 10^{-3}$ (dashed) and $Z_n(0) = 10^{-4}$ (solid). The finite-time blow-up occurs later for smaller values of $Z_n(0)$ but has the same form.

The rate of propagation $\dot{Z}_n$ is determined by the zero stress-intensity condition (3.10): if the rate of propagation is too fast then the stress intensity will become negative; if it is too slow then the stress intensity will become positive. The stress intensity is linear in H, and the updated values of H after one time step are linear in $\dot{Z}_n$. Hence the change in stress intensity is linear in $\dot{Z}_n$. Thus, by time stepping (4.1) using two trial values of $\dot{Z}_n$ and calculating the stress intensity in each case, we can calculate the value of $\dot{Z}_n$ that gives zero stress intensity and in this way determine the correct rate of propagation $\dot{Z}_n(\tau)$. The value of Z_n was also updated using an explicit Euler time step.

As an initial condition, we generally chose a crack length $Z_n = 10^{-4}$ and an initial profile $H = C(1-\zeta)^{2/3}$, where C was chosen to give $P(0) = 1$. The results described below were obtained with $N = 100$.

4.2. *Numerical results*

We commence by examining the rate of propagation. Figure 2 plots the dimensionless crack length Z_n against τ and shows that Z_n grows at an ever increasing rate. The length approaches infinity with a finite-time blow-up at $\tau = \tau^*$, where τ^* depends on the initial conditions. For example, the blow-up time τ^* is increased from 14 if $Z_n(0) = 10^{-1}$ to 52 if $Z_n(0) = 10^{-3}$ and to 71 if $Z_n(0) = 10^{-4}$, but it occurs at approximately the same time interval after $Z_n(\tau)$ reaches $Z_n = 1$. A logarithmic plot of the crack speed $\dot{Z}_n$ against length Z_n (figure 3) shows that the propagation has two regimes: for small crack lengths ($Z_n \ll 1$) the results suggest that $\dot{Z}_n \sim Z_n$, which gives exponential growth; for large crack lengths ($Z_n \gg 1$) the results suggest that $\dot{Z}_n \sim Z_n^2$, which gives rise to the observed finite-time blow-up, since integration of $\dot{Z}_n = \lambda Z_n^2$ gives $Z_n = \lambda/(\tau^* - \tau)$.

Some insight into the two regimes of propagation is obtained by examining the shape of the crack (figure 4) and the pressure distribution (figure 5). Recall from (3.2) and (3.5) that both H and ζ are scaled with $z_n(t)$ so that the physical width and

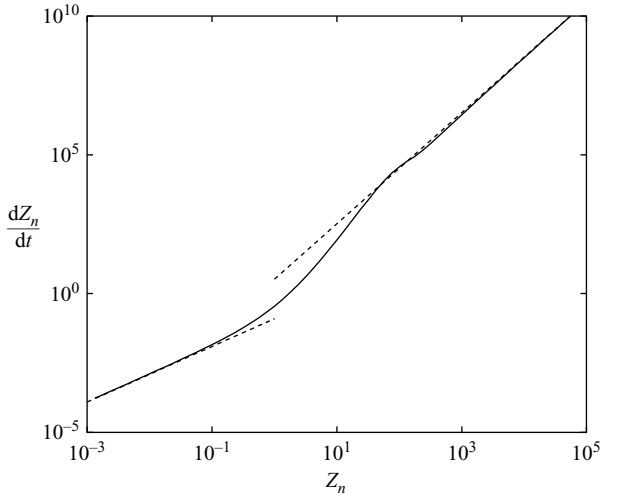

FIGURE 3. Logarithmic plot of the propagation rate $dZ_n/d\tau$ against Z_n showing a change of regime when $Z_n = O(1)$. The theoretical predictions for small and large crack lengths (dashed lines) have slopes 1 and 2 respectively and intercepts given by the detailed analyses in § 5 and § 6.

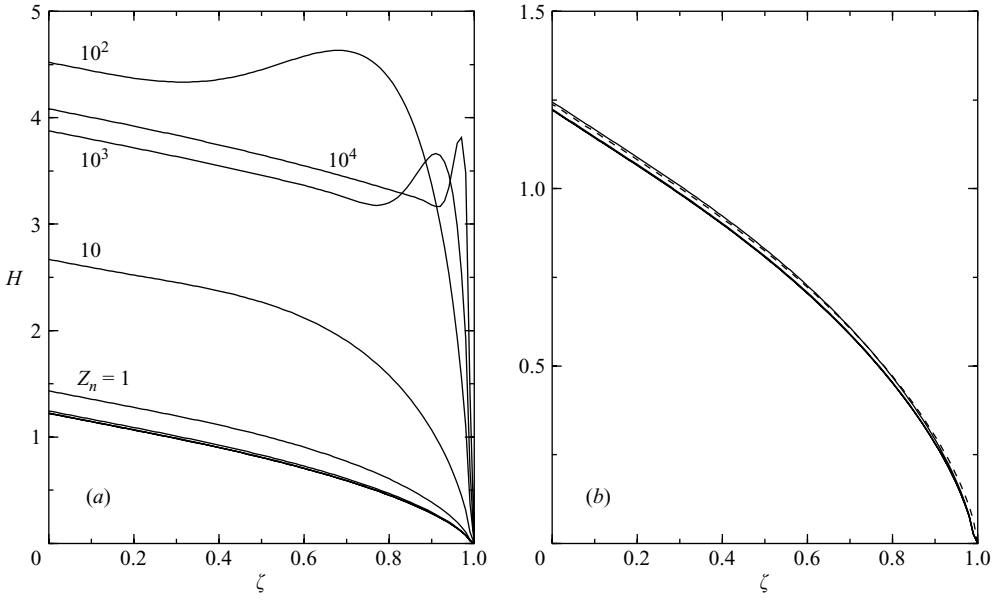

FIGURE 4. (*a*) Plot of the half-width H against ζ at lengths $Z_n(\tau) = 10^{-4}$, 10^{-3}, 10^{-2}, 10^{-1}, 1, 10, 10^2, 10^3 and 10^4 for $Z_n(0) = 10^{-5}$. (*b*) The half-width H for $Z_n = 10^{-4}$, 10^{-3}, 10^{-2} and 10^{-1} together with the theoretical similarity solution for short crack lengths (dashed).

length are both proportional to $Z_n(\tau)$, which increases by orders of magnitude during the times shown in figure 4.

For early times, when $Z_n \ll 1$, figure 4(*a*) suggests that the growth is self-similar, as the shape $H(\zeta)$ collapses for $10^{-4} \leqslant Z_n \leqslant 10^{-2}$. For these early times the pressure decreases monotonically from $P(0)$ towards a negative singularity at the crack tip

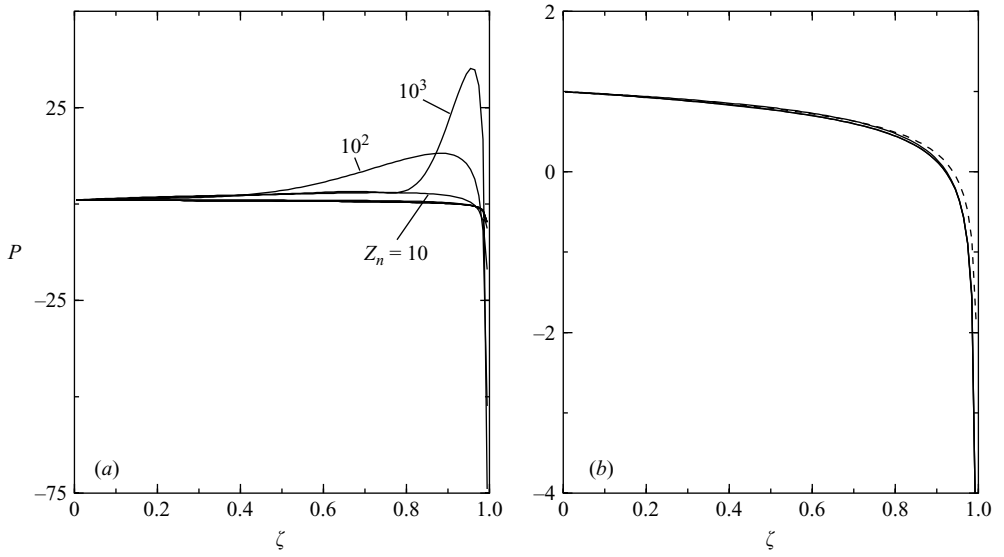

FIGURE 5. (*a*) Plot of the elastic pressure P against ζ at lengths $Z_n(\tau) = 10^{-3}$, 10^{-2}, 10^{-1}, 1, 10, 10^2 and 10^3 for $Z_n(0) = 10^{-4}$. (*b*) The profiles for $Z_n = 10^{-4}$, 10^{-2}, 10^{-1} and 1 together with the theoretical similarity solution for short crack lengths (dashed).

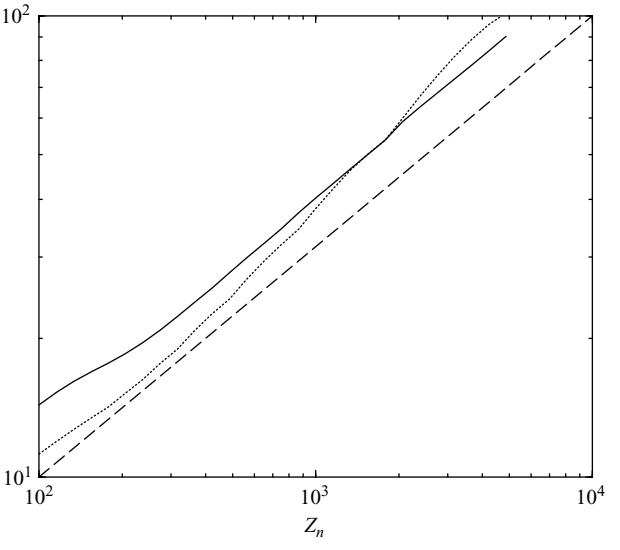

FIGURE 6. Logarithmic plot of the maximum pressure in the head $P_{\max}$ (solid) and its distance from the tip $Z_n(1 - \zeta(P_{\max}))$ (dotted) against Z_n for $Z_n \gg 1$. Both variables seem to scale roughly like $Z_n^{1/2}$ (dashed).

(figure 5*b*). A self-similar solution for small crack lengths is derived in § 5 using asymptotic methods to extract the singularity in pressure at the crack tip.

For later times, when $Z_n \gg 1$, figure 4 suggests that the solution develops a head region, which occupies a decreasing fraction of the crack's length but grows in length when the solution is scaled back to the physical variables, and a tail region. Figure 5(*a*) shows that the pressure profile for $Z_n = 10^2$ and $Z_n = 10^3$ remains $O(1)$ in the tail region and has a maximum, which increases with Z_n, in the head region. Figure 6

shows that the maximum pressure and the rescaled distance of the maximum pressure from the crack tip both behave like $Z_n^{1/2}$. This suggests that the elastic pressure gradient in the head is $O(1)$, comparable to buoyancy, as in the solutions derived for steady propagation in Lister (1990*b*). A similarity solution for the tail region, which is matched asymptotically to a solution for the head, is presented in § 6.

5. Early times: crack length ≪ buoyancy length

In section § 4 we noted that in the early stages of propagation, when the crack length is much less than the buoyancy length ($Z_n \ll 1$), the crack grows exponentially and with an approximately constant scaled shape $H(\zeta)$ – suggesting self-similar behaviour. We now find the appropriate self-similar solution to equations (3.6)–(3.10) and compare it with the time-dependent calculations. We also make some comparison with previous solutions in Spence & Sharp (1985).

For $Z_n \ll 1$ we may neglect the $O(1)$ buoyancy compared with the much larger $O(Z_n^{-1})$ elastic pressure gradient in (3.6). We seek a solution in which $\dot{Z}_n = \lambda Z_n$ and $\partial H/\partial \tau = 0$, which seems reasonable from the results of § 4. Under these assumptions (3.6) and (3.8) become

$$\lambda \left(H - \zeta \frac{\partial H}{\partial \zeta} \right) = \frac{1}{3} \frac{\partial}{\partial \zeta} \left(H^3 \frac{\partial P}{\partial \zeta} \right), \tag{5.1}$$

$$3\lambda = -\lim_{\zeta \to 1} H^2 \frac{\partial P}{\partial \zeta}. \tag{5.2}$$

We wish to solve for the scaled half-width H, pressure P and propagation rate λ. We remove the dependence on λ from the equations by rescaling $f = H\lambda^{-1/3}$ and $g = P\lambda^{-1/3}$ to obtain

$$f - \zeta \frac{\mathrm{d}f}{\mathrm{d}\zeta} = \frac{1}{3} \frac{\mathrm{d}}{\mathrm{d}\zeta} \left(f^3 \frac{\mathrm{d}g}{\mathrm{d}\zeta} \right), \tag{5.3}$$

$$g(\zeta) = -\frac{1}{\pi} \int_0^1 \frac{\mathrm{d}f}{\mathrm{d}s} k(s, \zeta)\, \mathrm{d}s, \tag{5.4}$$

$$\lim_{\zeta \to 1} f^2 \frac{\mathrm{d}g}{\mathrm{d}\zeta} = -3, \tag{5.5}$$

$$f(1-\zeta)^{-1/2} \to 0 \quad \text{as } \zeta \to 1. \tag{5.6}$$

The solution to these equations gives the propagation rate from

$$\lambda = \frac{1}{g(0)^3}. \tag{5.7}$$

Equations (5.3)–(5.6) are solved numerically.

Spence & Sharp (1985) derived equations governing symmetric propagation of a crack with no buoyancy in an infinite elastic solid, fed by a flux with given time-dependence. For fluxes of the form $Q = At^\alpha$ and $Q = A\mathrm{e}^{\alpha t}$ equations similar to (5.3)–(5.6) were obtained, the differences being the numerical coefficients in (5.3) and the use of the symmetric kernel (2.7) instead of (2.8) in (5.4). Spence & Sharp (1985) considered propagation for a range of values of α, which led them to derive similarity solutions in which the critical stress intensity was a function of time. (A time-dependent critical stress intensity is not physically realistic, and so these solutions are strictly only relevant in the cases where $K = 0$.) In particular, the special case

$K = 0$ was investigated for a flux $Q = At$, and we use this case as a test to validate our numerical scheme for the solution of (5.3)–(5.6). We also present results for the case of a symmetric crack with constant source over-pressure and $K = 0$, which was not studied in Spence & Sharp (1985).

5.1. *Numerical scheme*

Numerical solution for the scaled width f is aided by accounting for the singularities in f and the scaled pressure g near the tip. As outlined in the Appendix, the near-tip singularities for a fluid-driven crack with $K = 0$ take the form $f \sim A(1-\zeta)^{2/3}$ and $g \sim B(1-\zeta)^{-1/3}$ where A and B are known, related constants (Spence & Sharp 1985). Thus we write

$$f(\zeta) = (1-\zeta)^{2/3} F(\zeta), \tag{5.8}$$

$$g'(\zeta) = (1-\zeta)^{-4/3} G(\zeta), \tag{5.9}$$

and solve for F and G, which are non-zero at $\zeta = 1$ as we have extracted the behaviour of f and g' as $\zeta \to 1$. With F assumed to be finite at the tip the solution will then satisfy (5.6) automatically and the singularity in pressure is dealt with exactly.

In order to avoid calculating second derivatives of the pressure we integrate (5.3) using the boundary conditions (5.5) and (5.6) to give

$$-2\int_{\zeta}^{1} f(s)\,\mathrm{d}s = \zeta f + \frac{1}{3} f^3 \frac{\mathrm{d}g}{\mathrm{d}\zeta}. \tag{5.10}$$

Writing $\xi = 1 - \zeta$ and substituting from (5.8) and (5.9), we obtain

$$2\xi^{-2/3}\int_{0}^{\xi} s^{2/3} F(s)\,\mathrm{d}s = (1-\xi)\,F + \frac{1}{3}F^3 G, \tag{5.11}$$

which we solve using a Newton method.

For the Newton method the function F is approximated using a quadratic spline through N values of F at the mid-points of equally spaced panels. The transformed pressure gradient G is calculated from (5.4), the integrals of the spline being done analytically. A good initial guess for the Newton iteration is $F = A$, the coefficient in the near-tip asymptotic form of f, and it was found that the solution converged within 5 iterations.

Two tests were performed to verify the accuracy of the numerical scheme. By considering the difference between the value of F at the tip in the converged solution and the known value A from asymptotic analysis, we can estimate the accuracy of our numerical scheme as $O(1/N)$ (figure 7). Spence & Sharp (1985) studied the case of a symmetric crack fed by a constant flux of fluid with $K = 0$ and found that the half-width at the origin is 1.152. Using our numerical method on this problem, with $N = 100$, we find that the half-width at the origin is 1.149, which is in close agreement.

5.2. *Results*

Figure 8 shows the scaled half-width $f(\zeta)$ and pressure $g(\zeta)$ for $N = 100$. This solution gives $g(0) \approx 2.003$ which, from (5.7), corresponds to a growth rate $\lambda \approx 0.124$. Having found the similarity solution, we compare with the numerical results of § 4 for $Z_n \ll 1$. The dashed curve in figure 4(*b*) is the similarity solution, which is in very good agreement with the time-dependent numerical results, within about 2 % for $Z_n \leqslant 0.1$. The dashed line in figure 3 corresponds to the theoretical prediction

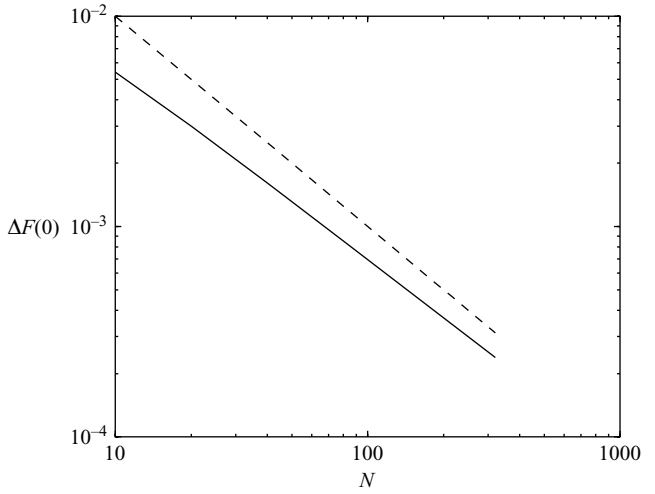

FIGURE 7. Logarithmic plot of the error (solid) in the tip value of F in numerical solutions of (5.11) against the number of panels N, suggesting decay like N^{-1} (dashed).

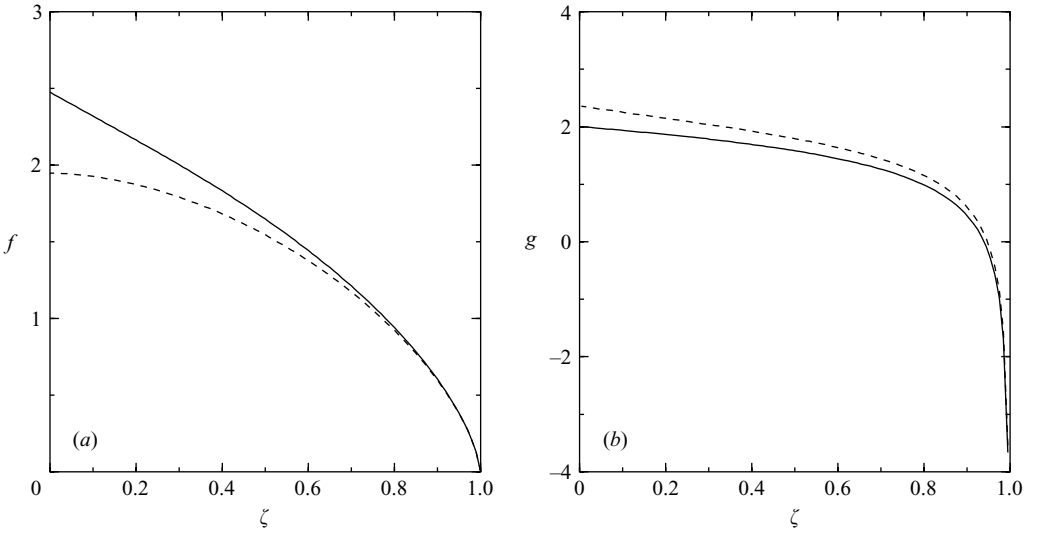

FIGURE 8. Plot of the similarity solutions of (5.3)–(5.6) for $Z_n \ll 1$: (*a*) scaled half-width $f(\zeta)$ and (*b*) scaled pressure $g(\zeta)$ for $N = 100$. The solid line is for the kernel (2.8) and the dashed line is for the kernel (2.7).

for the relationship between Z_n and $\dot{Z}_n$, and the agreement with the time-dependent numerical results is again very good for small crack lengths. The rate determined by fitting a straight line to the data obtained in § 4 over $10^{-3} \leqslant Z_n \leqslant 10^{-1}$ is $\lambda \approx 0.128$.

5.3. *Symmetric crack driven by over-pressure*

Using our numerical scheme we can also calculate the similarity solution for a symmetrically propagating crack with constant source over-pressure and $K = 0$. The solution is again characterized by exponential growth with growth rate λ. Figure 8 shows the rescaled crack half-width and pressure, which are the solutions to (5.3)–(5.6)

with the symmetric kernel (2.7) in (5.4). The rate of propagation is $\lambda = 0.0757$, so that a crack that propagates symmetrically in an infinite solid grows at a slower rate than a crack that propagates away from a traction-free boundary.

6. Late times: crack length $\gg$ buoyancy length

In § 4 we saw that during the later stages of propagation, when the crack length has greatly exceeded the buoyancy length ($Z_n \gg 1$), the rate of propagation behaves like $\dot{Z}_n = \lambda Z_n^2$, leading to a finite-time blow-up. The time-dependent calculations (figures 4, 5 and 6) show that the solution develops a head, where the elastic pressure gradient and buoyancy are both important, and a tail, where the flow is driven primarily by buoyancy. In this section we describe a similarity solution for the tail and match this to a solution for the head which is closely related to the solutions obtained by Lister (1990*b*) for steady buoyancy-driven propagation.

6.1. *The tail region*

For $Z_n \gg 1$ the elastic pressure gradient is $O(Z_n^{-1})$ and hence small compared with buoyancy except in a short region of decreasing size $O(Z_n^{-1/2})$ near the crack tip $\zeta = 1$ (figure 5). We derive a solution for the tail region by neglecting buoyancy in (3.6), setting $Z_n = \lambda Z_n^2$ (from figure 3) and searching for a similarity solution such that $\partial H/\partial \tau = 0$, which gives

$$\lambda \left(H - \zeta \frac{\partial H}{\partial \zeta} \right) = -\frac{1}{3} \frac{\partial}{\partial \zeta} (H^3). \tag{6.1}$$

This first-order differential equation can be integrated to give the family of solutions

$$\frac{H}{\lambda^{1/2}} = a + (a^2 - \zeta)^{1/2}. \tag{6.2}$$

These solutions have a non-zero width as $\zeta \to 1_-$, which must be matched to the head.

The constant a is determined from a boundary condition at $\zeta = 1_-$ based on an asymptotic balance of fluxes with the head. Since the head region occupies a decreasing proportion of the total volume, the flux condition (3.8) also applies to the limit $\zeta \to 1_-$ in the tail and not just to the crack tip. With this observation, we neglect the elastic pressure gradient in (3.8) to obtain

$$H(1) = (3\lambda)^{1/2}, \tag{6.3}$$

and deduce that $a = (4/3)^{1/2}$. We will need to match to this width when we examine the head in § 6.2.

Having obtained H, we use (3.7) to obtain

$$P(0) = \lim_{\zeta \to 0} \frac{\lambda^{1/2}}{2\pi} \int_0^1 \frac{k(s, \zeta)\, \mathrm{d}s}{\left(\frac{4}{3} - s\right)^{1/2}}. \tag{6.4}$$

By making the substitution $s = \zeta u$ and noting that $\zeta k(\zeta u, \zeta) = k(u, 1)$, we deduce that

$$P(0) = \frac{\lambda^{1/2}}{2\pi} \left(\frac{3}{4} \right)^{1/2} \int_0^\infty k(u, 1)\, \mathrm{d}u = \frac{(3\lambda)^{1/2}}{\pi}. \tag{6.5}$$

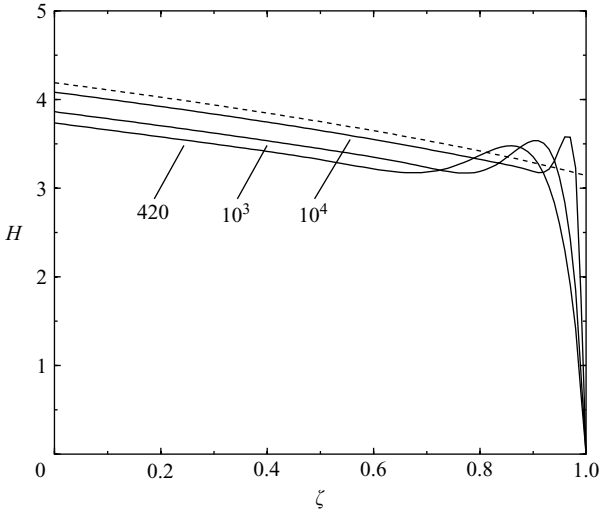

FIGURE 9. Plot of the half-width H against ζ for lengths $Z_n = 420$, 10^3 and 10^4. The tail shows increasing agreement with the asymptotic solution (6.6) (dashed).

The boundary condition $P(0) = 1$ in (3.9) then determines the propagation rate as $\lambda = \pi^2/3$. Thus the solution for the tail is

$$H = \frac{2\pi}{3}\left(1 + \left(1 - \frac{3\zeta}{4}\right)^{1/2}\right). \tag{6.6}$$

We compare the asymptotic propagation rate and shape of the tail derived above with the numerical results of § 4. Figure 3 shows that the theoretical prediction $\dot{Z}_n = \pi^2 Z_n^2/3$ agrees very well with the numerical simulation for $Z_n \gg 1$. Figure 9 shows that the half-width of the tail tends towards (6.6) as the crack length Z_n increases. The rate of convergence is consistent with an $O(Z_n^{-1/2})$ correction term, as might be expected from the length of the head.

6.2. *The head region*

As noted in figure 6, the head occupies a small fraction of the crack's length so that the time to propagate the length of the head is much shorter than the time taken to propagate the length of the crack. This separation of time scales suggests that the head can adjust relatively rapidly to changing conditions in the tail and thus we should consider quasi-steady solutions in the frame of the head.

The half-width at the front of the tail was found in (6.3) to be $(3\lambda)^{1/2}$, and the width decreases from this value to 0 over the length of the head. If we write the scale of the head as L, then we estimate $\partial H/\partial\zeta$ as $(3\lambda)^{1/2}/L$. From (3.7) the elastic pressure also scales like $(3\lambda)^{1/2}/L$ and thus the pressure gradient scales like $(3\lambda)^{1/2}/L^2$. If the elastic pressure gradient and buoyancy are to balance in (3.6), then $L \sim (3\lambda)^{1/4} Z_n^{-1/2}$ and $P \sim (3\lambda)^{1/4} Z_n^{1/2}$. This dependence on Z_n agrees with the observed behaviour of $P_{\max}$ and the length of the head in figure 6.

Motivated by these scalings, we define

$$\xi = \frac{1-\zeta}{L}, \tag{6.7}$$

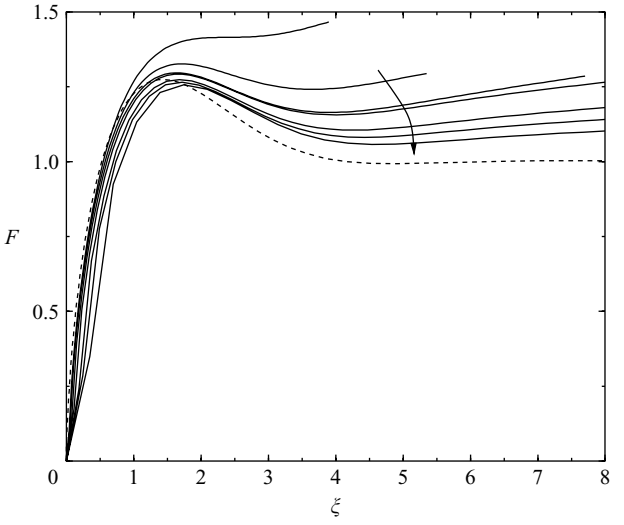

FIGURE 10. Plot of the scaled head shapes $F(\xi) = H/(3\lambda)^{1/2}$ against scaled distance from the tip $\xi = (1-\zeta)(3\lambda)^{-1/4} Z_n^{1/2}$, for Z_n in (50, 5000). The arrow shows the direction of increasing Z_n. The dashed curve is the solution for steady propagation at $K = 0$ found in Lister (1990*b*).

$$F(\xi) = \frac{H}{(3\lambda)^{1/2}}, \tag{6.8}$$

$$G(\xi) = \frac{PL}{(3\lambda)^{1/2}}, \tag{6.9}$$

where $L = (3\lambda)^{1/4} Z_n^{-1/2}$. In the limit of large Z_n, the assumption of a quasi-steady solution yields the following set of equations:

$$\frac{\partial F}{\partial \xi} = \frac{\partial}{\partial \xi}\left(F^3\left(\frac{\partial G}{\partial \xi} + 1\right)\right), \tag{6.10}$$

$$G = -\frac{1}{\pi}\int_0^\infty \frac{\partial F}{\partial s}\frac{1}{s-\xi}\,\mathrm{d}s, \tag{6.11}$$

$$\lim_{\xi\to 0} F^2\left(1 + \frac{\partial G}{\partial \xi}\right) = 1, \tag{6.12}$$

$$F\xi^{1/2} \to 0 \quad \text{as } \xi \to 0. \tag{6.13}$$

Integrating (6.10) and applying (6.12) gives

$$\frac{\partial G}{\partial \xi} = \frac{1}{F^2} - 1. \tag{6.14}$$

Equations (6.14), (6.11) and (6.13) are precisely those solved numerically by Lister (1990*b*) to describe buoyancy-driven crack propagation at a critical stress intensity $K = 0$. The solution consists of a bulge near the crack tip after which the half-width tends to $F = 1$ as $\xi \to \infty$. In figure 10 the time-dependent half-width of the head calculated in § 4 has been rescaled according to (6.7)–(6.9) and we see an approximate and improving collapse to the solution obtained by Lister (1990*b*). The resolution of the head becomes worse as Z_n increases because the size of the head decreases like $Z_n^{-1/2}$ and we have used a fixed grid.

7. Discussion

We have obtained solutions in different regimes for buoyancy-driven fluid fracture of a two-dimensional crack that propagates with constant source over-pressure away from a traction-free boundary. The form of the solution depends on the length of the crack relative to the buoyancy length $\Delta P/\Delta\rho g$, which measures the relative importance of the elastic pressure gradient and buoyancy. The solutions found here have some features in common with purely pressure-driven and purely buoyancy-driven crack propagation, but the introduction of buoyancy and over-pressure simultaneously has led to new effects particularly when the length of the crack exceeds the buoyancy length.

For both short cracks, when the length is less than the buoyancy length, and large cracks, when the length is greater than the buoyancy length, the over-pressure at the source acts to make the width of the crack grow in proportion its length. The growth in width leads to a rapid increase in the flux, which, from lubrication theory is proportional to the cube of the width. The driving force for the flux is dominated either by the elastic pressure gradient for short cracks or by buoyancy for large cracks. For the case of short cracks, we have shown that the crack growth is exponential and obtained a similarity solution for the crack width and pressure profiles. This solution and the predicted growth rate agree with the time-dependent numerical simulations of the crack growth. The similarity solution is similar to the solutions derived by Spence & Sharp (1985) for various forms of non-buoyant crack growth in an infinite solid. For the case of large cracks we have identified a new behaviour in which crack growth accelerates towards a finite-time blow-up with the length increasing like $(t^* - t)^{-1}$, where t^* is the blow-up time. The solution in this regime develops a head-and-tail structure: in the tail the elastic pressure gradient is negligible and the flow is buoyancy-driven; in the head the elastic pressure gradient becomes comparable to buoyancy and acts to smooth the shock which would otherwise result from buoyancy-driven flow in the tail. We have derived an analytic solution for the tail, which is governed by a kinematic-wave equation. We have also derived the asymptotic governing equations for the head, and obtained an asymptotic matching to the tail by exploiting a quasi-steady analysis which reduces the problem to one solved in Lister (1990*b*). The analytical solutions derived for large lengths also agree well with the numerical simulations.

The solutions derived here contrast with those derived by Spence *et al.* (1987) and Lister (1990*b*), who considered steady propagation of a buoyant liquid-filled crack. These authors imposed a fixed flux as the boundary condition at the base of the crack, which meant the pressure decayed like the reciprocal of the distance from the head. The difference here is that the constant over-pressure ΔP leads to a rapidly increasing width and flux. Mériaux & Jaupart (1998) obtained numerical solutions for the width of a crack propagating with buoyancy and over-pressure in a finite elastic plate. Their results showed that the crack widened at the base and developed a head, with the crack growth accelerating in time. See in particular figures 12 and 15 in Mériaux & Jaupart (1998). Our analysis has demonstrated that these features develop primarily because of the interaction between buoyancy and over-pressure, with the finite thickness of the solid plate playing a secondary role.

The assumptions underlying the formulation of the problem presented here must be re-examined as the crack accelerates towards a finite-time blow-up. Various additional effects may start to play a role, some of which can regularize the problem. Firstly, both the width and the rate of propagation of the crack increase so that, even though

the crack remains long and thin (the aspect ratio scales like the ratio of over-pressure ΔP and elastic modulus m), the Reynolds number increases as the crack grows. Eventually this leads to turbulent flow in the crack and the expression relating the flux of fluid q to the pressure gradient and width must be modified (e.g. Lister & Kerr 1991, equations 8*b* and 8*c*). While this changes the exponent α in $\dot{Z}_n \sim Z_n^\alpha$, it is still the case that $\alpha > 1$, resulting in blow-up. A second consequence of the increasing crack speed is that the tip speed eventually becomes comparable with the Rayleigh wave speed in the solid. At this stage the assumption of elastostatics must be abandoned and we must reformulate the problem in terms of elastodynamics, where the kinetic energy of the solid is comparable to the strain energy of the crack. Scaling arguments suggest that this prevents blow-up, though this remains to be confirmed by calculation.

Three modifications may arise from the geometry of the problem. Throughout the analysis presented here, we have assumed that the vertical extent z_n of the crack is less than the horizontal (along-strike) extent, which allows us to model the dyke as two-dimensional. When the crack reaches a length comparable to the horizontal extent of the crack the elastic relation (2.6) will change to reflect the three-dimensional nature of the crack (e.g. Lister 1990*a*). Both lateral and vertical propagation must then be considered. Another consideration connected to the size of the crack is the presence of a free surface (e.g. the Earth's surface) through which the crack may break; this changes the kernel in (2.6) and a numerical study of this effect has been undertaken in Mériaux & Jaupart (1998). A further consideration is the flux of fluid into the crack, which would also blow up in finite time if the over-pressure were maintained. In practice, however, a large flux would lead to the source being evacuated and a reduction in over-pressure at the base of the crack. All these additional effects lead to interesting extensions of this work and would provide further insight into the geological problem of how magma is fed through the crust.

In conclusion, we have included buoyancy in the model of an over-pressured dyke propagating through the Earth's crust. The inclusion of buoyancy has led to a new behaviour, which we have explained through asymptotic analysis of the governing integral and partial-differential equations. We have derived new solutions governing this regime of dyke propagation and highlighted connections to other studies. There is a wide variety of extensions to this work which will provide interesting mathematical problems and further insight into dyke propagation.

Appendix. Asymptotic form for f and g at $\zeta = 1$

Near the crack tip we pose $f(s) = A(1-s)^\alpha$ and use

$$g(\zeta) = -\frac{1}{\pi}\int_0^1 k(s,\zeta)\frac{\mathrm{d}f}{\mathrm{d}s}\,\mathrm{d}s \tag{A 1}$$

to calculate the pressure near the crack tip. Following Spence & Sharp (1985) we write $s = 1-(1-\zeta)u$ so that $f = A(1-\zeta)^\alpha u^\alpha$. Near the tip the kernel is dominated by $1/(s-\zeta)$ and, substituting into (A 1), we obtain

$$g(\zeta) \sim (1-\zeta)^{\alpha-1}\frac{\alpha A}{\pi}\int_0^\infty \frac{u^{\alpha-1}}{1-u}\,\mathrm{d}u, \tag{A 2}$$

$$g'(\zeta) \sim -(1-\zeta)^{\alpha-2}\frac{\alpha(\alpha-1)A}{\pi}\int_0^\infty \frac{u^{\alpha-1}}{1-u}\,\mathrm{d}u. \tag{A 3}$$

By integrating the function $z^{\alpha-1}/(1-z)$ around a 'keyhole' contour it is easy to show that

$$\int_0^\infty \frac{u^{\alpha-1}}{1-u}\,\mathrm{d}u = \pi\cot\pi\alpha. \tag{A 4}$$

Using these results and balancing $-\zeta f'$ with $(f^3 g')'/3$ in (5.3), we obtain the following equation governing the form of f at the crack tip:

$$3 = A^3\,(1-\zeta)^{3\alpha-2}\,\alpha\,(\alpha-1)\cot\pi\alpha. \tag{A 5}$$

This gives $\alpha = 2/3$ and $A^3 = 27\sqrt{3}/2$, in agreement with Spence & Sharp (1985). For the case $K \neq 0$ near the tip, we have $f(s) \sim K\,(1-s)^{1/2}$ which gives $g'(s) \sim -K^{-2}\,(1-s)^{-1}$ and, on integration, we obtain $g(s) \sim K^{-2}\log(1-s)$.

REFERENCES

Adachi, J. I. & Detournay, E. 2002 Self-similar solution of a plane-strain fracture driven by a power-law fluid. *Intl J. Numer. Anal. Meth. Geomech.* **26**, 579–604.

Atkinson, C. & Craster, R. V. 1991 Plane strain fracture in poroelastic media. *Proc. R. Soc. Lond.* A **434**, 605–633.

Atkinson, C. & Thiercelin, M. 1993 The interaction between the wellbore and pressure-induced fractures. *Intl J. Frac.* **59** (1), 23–40.

Bolchover, P. & Lister, J. R. 1999 The effect of solidification on fluid-driven fracture, with application to bladed dykes. *Proc. R. Soc. Lond.* A **455**, 2389–2409.

Broberg, K. B. 1999 *Cracks and Fracture*. Academic.

Garagash, D. I. & Detournay, E. 1998 Similiarity solution of a semi-infinite fluid-driven fracture in a linear elastic solid. *C. R. Acad. Sci. Paris* IIb, **326**, 285–292.

Geertsma, J. & Haafkens, R. 1979 A comparison of the theories for predicting width and extent of vertical hydraulically induced fractues. *J. Energy Resour. Technol.* **101**, 8–19.

Huang, N. C., Szewczyk, A. A. & Li, Y. C. 1990 Self-similar solution in problems of hyrdaulic fracturing. *Trans. ASME: J. Appl. Mech.* **57**, 877–881.

Ito, G. & Martel, S. J. 2002 Focusing of magma in the upper mantle through dike interaction. *J. Geophys. Res.* **107** (B10) art. no. 2223.

Lawn, B. R. & Wilshaw, T. R. 1975 *Fracture of Brittle Solids*. Cambridge University Press.

Lister, J. R. 1990*a* Buoyancy-driven fluid fracture: similairty solutions for the horizontal and vertical propagation of fluid-filled cracks. *J. Fluid Mech.* **217**, 213–239.

Lister, J. R. 1990*b* Buoyancy-driven fluid fracture: the effects of material toughness and of low-viscosity precursors. *J. Fluid Mech.* **210**, 263–280.

Lister, J. R. 1994*a* The solidification of buoyancy-driven flow in a flexible-walled channel. Part 1. Constant-volume release. *J. Fluid Mech.* **272**, 21–44.

Lister, J. R. 1994*b* The solidification of buoyancy-driven flow in a flexible-walled channel. part 2. Continual release. *J. Fluid Mech.* **272**, 45–65.

Lister, J. R. & Kerr, R. C. 1991 Fluid-mechanical models of crack propagation and their application to magma transport in dykes. *J. Geophys. Res.* **96** (B6), 10049–10077.

Lorentz, H. A. 1907 A general theory concerning the motion of a viscous fluid. *Abhandl. Theoret. Phys.* **1**, 23.

Menand, T. & Tait, S. R. 2002 The propagation of a buoyant liquid-filled fissure from a source under constant pressure: An experimental approach. *J. Geophys. Res.* **107** (B11) art. no. 2306.

Mériaux, C. & Jaupart, C. 1998 Crack propagation through an elastic plate. *J. Geophys. Res.* **103** (B8), 18295–18314.

Muller, J. R., Ito, G. & Martel, S. J. 2001 Effects of volcano loading on dike propagation in an elastic half-space. *J. Geophys. Res.* **106** (B6), 11101–11113.

Nordgren, R. 1972 Propagation of vertical hydraulic fractures. *J. Petrol. Tech.* **253**, 306–314.

Perkins, T. & Kern, L. 1961 Widths of hyrdaulic fractures. *J. Petrol. Tech., Trans AIME* **222**, 937–949.

Rubin, A. M. 1995*a* Getting granite dikes out of the source region. *J. Geophys. Res.* **100** (B4), 5911–5929.

Rubin, A. M. 1995*b* Propagation of magma-filled cracks. *Annu. Rev. Earth Planet. Sci.* **23**, 287–336.

Rubin, A. M. 1998 Dike ascent in partially molten rock. *J. Geophys. Res.* **103** (B9), 20901–20919.

Spence, D. A. & Sharp, P. 1985 Self-similar solutions for elastohydrodynamic cavity flow. *Proc. R. Soc. Lond.* A **400**, 289–313.

Spence, D. A., Sharp, P. & Turcotte, D. L. 1987 Buoyancy-driven crack propagation: a mechanism for magma migration. *J. Fluid Mech.* **174**, 135–153.

Weertman, J. 1971 Theory of water-filled crevasses in glaciers applied to vertical magma transport beneath oceanic ridges. *J. Geophys. Res.* **76** (5), 1171–1183.